Biologically effective dose in fractionated molecular radiotherapy-application to treatment of neuroblastoma with (131)I-mIBG.

Minguez Gabina, Pablo; Gustafsson, Johan Ruben; Flux, Glenn; Sjögreen Gleisner, Katarina

Published in:
Physics in Medicine and Biology

DOI:
10.1088/0031-9155/61/6/2532

2016

Document Version:
Peer reviewed version (aka post-print)

Biologically effective dose in fractionated molecular radiotherapy – application to treatment of neuroblastoma with ^{131}I-mIBG

Pablo Mínguez[1,2] , Johan Gustafsson[1], Glenn Flux[3] and Katarina Sjögreen Gleisner[1]

[1]Department of Medical Radiation Physics, Clinical Sciences Lund, Lund University, 22185 Lund, Sweden
[2]Department of Medical Physics, Gurutzeta/Cruces University Hospital, 48903 Barakaldo, Spain
[3]Joint Department of Physics, Royal Marsden NHS Foundation Trust & Institute of Cancer Research, Sutton SM2 5PT, UK

E-mail: pablo.minguezgabina@osakidetza.eus

Abstract

In this work, the biologically effective dose (BED) is investigated for fractionated molecular radiotherapy (MRT). A formula for the Lea-Catcheside G-factor is derived which takes the possibility of combinations of sub-lethal damage due to radiation from different administrations of activity into account. In contrast to the previous formula, the new G-factor has an explicit dependence on the time interval between administrations. The BED of tumour and liver is analysed in MRT of neuroblastoma with ^{131}I-mIBG, following a common two-administration protocol with a mass-based activity prescription. A BED analysis is also made for modified schedules, when due to local regulations there is a maximum permitted activity for each administration. Modifications include both the simplistic approach of delivering this maximum permitted activity in each of the two administrations, and also the introduction of additional administrations while maintaining the protocol-prescribed total activity. For the cases studied with additional (i.e. more than two) administrations, BED of tumour and liver decreases at most 12% and 29%, respectively. The decrease in BED of tumour is however modest compared to the two-administration schedule using the maximum permitted activity, where the decrease compared to the original schedule is 47%.

1. Introduction

Currently in molecular radiotherapy (MRT), there is an increasing interest in exposure parameters based on radiobiological models, which are believed to have the potential to better predict the effect of the treatment than absorbed dose alone (Barone *et al.* 2005; Dewaraja *et al.*, 2010; Strigari *et al.*, 2010; Strigari *et al.*, 2011; Strigari *et al.*, 2014). The most commonly used quantity is the biologically effective dose (BED), a radiobiological concept which was first introduced with a different name by Barendsen (1982) and was later renamed BED by Fowler (1989). The BED of a given treatment is defined as the hypothetical absorbed dose required to obtain the same biological effect if given with infinitesimal fractions or, for the case of protracted irradiation, with infinitely low absorbed-dose rate (Barendsen, 1982; Fowler, 1989). One aspect of BED is that it can be used to compare treatments given with different irradiation time-patterns with respect to the expected radiobiological response of tissues (Dale, 1990; Fowler, 1990; Howell *et al.*, 1994; Dale and Carabe-Fernandez, 2005; Cremonesi *et al.*, 2008). Since tumour and normal tissues typically respond differently to changes in the absorbed-dose rate or fractionation schedule, the irradiation time-pattern can be optimised using BED calculations (Dale, 1986; Millar, 1991).

For fractionated external beam radiotherapy (EBRT), the most commonly used expression for BED relies on the assumption that the time intervals between two consecutive fractions are long compared to repair half-times, so that sublethal damage repair can be considered to be effectively complete between fractions (Fowler, 1989). The total BED is then the sum of the BED of each fraction, that is, BED is linearly additive. For fractionated MRT, i.e. MRT given in several administrations of activity, it has also been assumed that the BED is linearly additive (Cremonesi *et al.*, 2006; Baechler *et al.*, 2008; Cremonesi *et al.*, 2008). However, this assumption is not valid when administrations are performed close in time, so that there is an appreciable interplay between the absorbed-dose rate curves corresponding to different administrations, i.e. when there are sublethal damages caused by the absorbed-dose rate curves resulting from different administrations that can combine into lethal damages. In order to analyse such fractionated schedules of activity delivery, the equations used to calculate BED need to be further developed.

Fractionated MRT may be studied for several reasons. When the primary organ at risk is a late-responding tissue, fractionation in EBRT is known to give a tissue sparing effect. This gives the possibility to increase tumour BED while keeping normal tissue BED constant, as explored in MRT for ^{90}Y-microsphere radioembolisation treatment of hepatic lesions (Cremonesi *et al.*, 2008). Another reason to introduce fractionation may be for legal considerations, when treatment centres have a licence that specifies a maximum authorised activity for a radionuclide to be stored or handled in the facility. This limits the activity to administer for the heavier patients in treatments prescribed based on patient mass (Otte *et al.*, 1999; Yanik *et al.*, 2002; Gedik *et al.*, 2008). Yet another reason may be the practical handling of high prescribed activities, in view of the radiological safety of staff, for which fractionation may be a feasible way to reduce the

effective dose to individual workers. A fourth reason to introduce fractionation may be absorbed-dose planning during the first administration to be used in subsequent administrations. One particular example of fractionated MRT is the treatment of neuroblastoma (NB) with ^{131}I-metaiodobenzylguanidine (mIBG) following the schedule by Gaze *et al.* (2005). In this schedule, two administrations separated by a fortnight are given, where the first is prescribed as activity per body mass (444 MBq/kg), and the second is tailored to deliver a whole-body absorbed dose of 4 Gy in total for the two administrations. Being designed as a myelo-ablative treatment, stem-cell harvesting is included in this schedule and stem-cell rescue is performed at approximately four weeks after the first administration. Generally in treatments with ^{131}I-mIBG, liver uptake is significant (Koral *et al.*, 2008) and possible liver toxicity has been addressed in NB treatments (Quach *et al.*, 2011).

The motivation of this work was a clinical treatment of NB at the Gurutzeta-Cruces University Hospital, where a patient was treated compassionately with ^{131}I-mIBG. The patient mass was 63 kg, which according to the protocol by Gaze *et al.* (2005) implied an administered activity of 28 GBq for the first administration, and assuming that the whole-body absorbed dose would be close to 2 Gy (Minguez *et al.*, 2015), another 28 GBq for the second administration. However, since the maximum authorised ^{131}I activity at the Gurutzeta-Cruces University Hospital is 14.8 GBq, a modification of the schedule was necessary. In practice, two administrations below the permitted level were given, similarly to what was carried out by Sudbrock *et al.* (2010). An alternative way, that would have allowed for maintaining the protocol-prescribed total activity and thus the whole-body absorbed dose, as well as not interfering with the stem-cell rescue, would be to divide the activity into multiple administrations distributed over the two-week time frame allocated for each of the two original administrations. Since a modification of the schedule of activity delivery results in a change in the delivered BED, it is of interest to elucidate the magnitude of the changes.

In this work, an expression for calculating BED in fractionated MRT is derived, which takes the interplay between sublethal damages resulting from absorbed-dose rate curves corresponding to different administrations into account. A general comparison between the expression derived in this study and that used in previous studies is performed. As an example application, BED is analysed for tumour and liver for the two-administration NB treatment schedule used in ^{131}I-mIBG following Gaze *et al.* (2005). Moreover, BED is analysed for schedules where additional fractionation is introduced for the purpose of complying with local regulations in situations when the patient mass infers an activity to administer which is above the maximum authorised activity, and for a two-administration schedule in which the maximum authorised activity is delivered.

2. Methods

2.1.Current BED expression in fractionated MRT

For protracted irradiation, such as in MRT, the BED at time *T* after the start of treatment is given by:

$$\mathrm{BED}(T) = D(T)\left(1 + \frac{D(T)}{\alpha/\beta}G(T)\right), \quad (1)$$

where α (Gy^{-1}) and β (Gy^{-2}) are the respective linear and quadratic radiosensitivity coefficients, $G(T)$ is a dimensionless function called the Lea-Catcheside G-factor (Lea and Catcheside, 1942) which takes the reduction in cell kill due to repair of sublethal damages during irradiation into account, and $D(T)$ is the absorbed dose, given by:

$$D(T) = \int_0^T R(t)\mathrm{d}t, \quad (2)$$

where $R(t)$ represents the absorbed-dose rate as a function of time.

Most often, repair is assumed to follow first-order kinetics and is modelled by a monoexponential function with rate constant μ. The function $G(T)$ is then given by (Kellerer and Rossi, 1974; Gustafsson *et al.*, 2013a):

$$G(T) = \frac{2}{D^2(T)}\int_0^T R(t)\left[\int_o^t \exp\big(-\mu(t-w)\big)\,R(w)\mathrm{d}w\right]\mathrm{d}t. \quad (3)$$

For MRT delivered in one administration, where $R(t)$ follows a monoexponential function with decay constant λ and the end of irradiation is considered to be infinity, then $\lim_{T\to\infty} G(T)$, here denoted as $G_{1,\infty}$ where the first subindex denotes the number of administrations, is given by:

$$G_{1,\infty} = \frac{\lambda}{\mu+\lambda}. \quad (4)$$

MRT can also be delivered in a number of administrations, *n* (fractionated MRT). For situations when the absorbed-dose rate curve has the same monoexponential behaviour in all administrations, previous publications (Cremonesi *et al.*, 2006; Baechler *et al.*, 2008; Cremonesi *et al.*, 2008) have given the following expression for BED:

$$\mathrm{BED} = \sum_{i=1}^{n} d_i\left(1 + \frac{d_i}{\alpha/\beta}\,G_{1,\infty}\right), \quad (5)$$

where d_i is the absorbed dose given during each administration. A particular case is that in which an equal amount of activity is given in all administrations, i.e. when $d_i = D/n$. Equation (5) then results in:

$$\mathrm{BED} = D\left(1 + \frac{D}{\alpha/\beta}\,\frac{1}{n}\,G_{1,\infty}\right). \qquad (6)$$

However, (5) and (6) are only valid for well-separated administrations so that the absorbed-dose rate curves associated with the individual administrations can be considered separately without interaction between them. Figure 1 shows an example of the absorbed-dose rate as a function of time when D is given in four administrations with a time interval between administrations, Δt, of 48 h, in which (6) would not be valid.

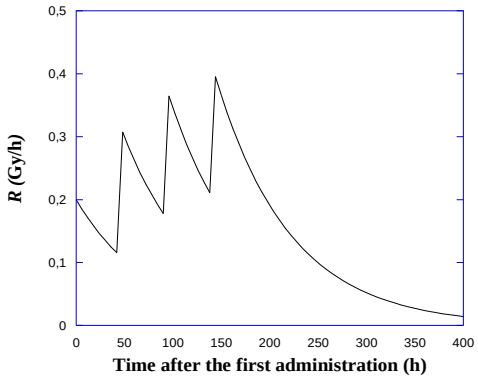

Figure 1. Absorbed-dose rate, R, as a function of time for four administrations separated by a Δt of 48 h.

As illustrated, the absorbed-dose rate used in the calculation of the G-factor depends not only on n, but also on Δt. Thus, the integrations in (3) should not be performed by viewing each administration independently, but need to take Δt into consideration.

Appendix A shows the derivation of $G_{n,\infty}$ for fractionated MRT given in n administrations with an equal amount of activity in each adminsitration.

2.2.Analysis of fractionated ^{131}I-mIBG treatment of NB

As starting point, we use data from the afore-mentioned NB patient. According to the schedule by Gaze *et al.* (2005), the patient mass of 63 kg implies an administered activity of approximately 28 GBq, given in two administrations separated by two weeks. In order to comply with the local regulations of a maximum of 14.8 GBq in each administration, different modifications of this schedule are analysed. In principle, such modification can be made in different ways, but a natural choice is to use equal amounts of activity and equal time intervals between administrations. Thus, the following schedules of activity delivery are considered: 1) two administrations each of 28 GBq separated by 336 h (2 weeks); 2) four administrations each of 14 GBq separated by 168 h (1 week); 3) six administrations each of 9.33 GBq separated by 112 h; 4) eight

administrations each of 7 GBq separated by 84 h and 5) two administrations each of 14.8 GBq separated by 336 h. Schedule 1 thus follows from the Gaze protocol, in schedules 2-4 the protocol-prescribed administered activity and timing of stem-cell rescue are maintained according to the protocol, and in schedule 5 only the locally-permitted maximum activity is given in each of the two administrations. Figure 2 illustrates the considered schedules of activity delivery.

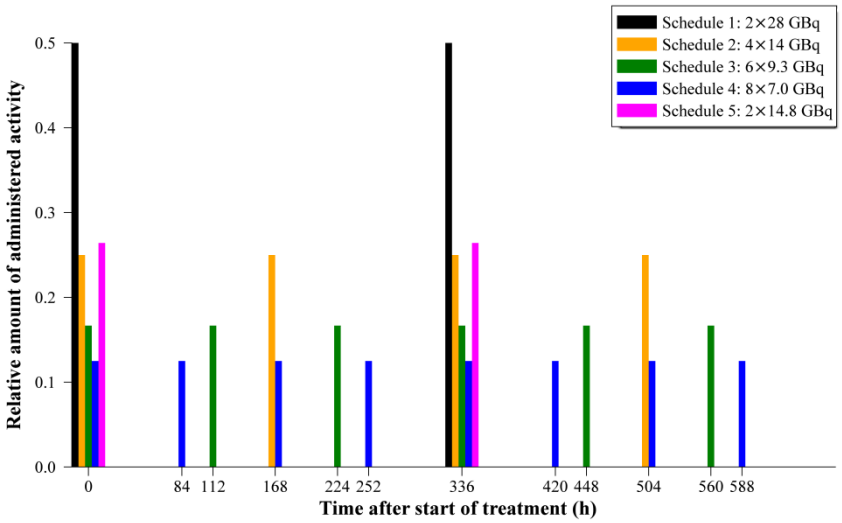

Figure 2. Schedules of activity delivery, including the protocol by Gaze *et al.* (2005) (Schedule 1:2×28 GBq), and the considered alternatives for decreasing the activity per administration (Schedule 2:4×14 GBq, Schedule 3:6×9.3 GBq, Schedule 4:8×7 GBq and Schedule 5:2×14.8 GBq).

For the further analysis representative dosimetric data are required, and are derived both from literature and from the afore-mentioned patient (see Appendix B). From the patient data for the liver, the absorbed dose per unit of administered activity, D/A_{Adm}, was obtained to 0.29 Gy/GBq and the effective decay constant (physical decay combined with biological washout), λ, to 0.009 h^{-1}. In Giammarile *et al.* (2008), D/A_{Adm}, was obtained to 0.83 Gy/GBq, and in Jacobsson *et al.* (1985), λ was obtained to 0.025 h^{-1}. It is worth noting that the liver ^{131}I-mIBG washout exhibits one fast and one slow phase (Koral *et al.*, 2008), and that data for the considered patient correspond to the slow phase, as estimated from late acquisition times. For tumour, reported values of D/A_{Adm} and λ in the same patient are few (Buckley *et al.*, 2007) and data from our patient study are therefore used, where D/A_{Adm} and λ obtained were 1.50 Gy/GBq and 0.008 h^{-1}, respectively. These values are within the ranges reported by Buckley *et al.* (2007).

Regarding radiobiological parameters, α/β values obtained *in vitro* for a variety of human NB cell lines have been reported. For instance, Courdi *et al.* (1992) reported a value of 1.85 Gy for the CHP100 cell line, Holmes *et al.* (1990) gave values of 5.00 Gy for the HX138 cell line and 9.38 Gy for the HX142 cell line, and Marchese *et al.* (1987) reported a value of 17.59 Gy for the SK-N-SH cell line. In Fertil and Malaise (1985), Malaise *et al.* (1987) and Amin *et al.* (1995), NB was included among highly responsive

tumours and values of 7.11 Gy, 8.31 Gy and 13.08 Gy were respectively reported. For the purpose of this study, the lowest and the highest α/β values found in the literature, i.e. 1.85 Gy and 17.59 Gy, respectively, are applied. For μ of tumour, values of 0.46 h^{-1} (Amin *et al.*, 1995) and of 1.28 h^{-1} (Brenner and Hall, 1991), have been reported, and both values are used for calculations. The pair of radiobiological parameters (α/β=1.85 Gy, and μ=0.46 h^{-1}) is used to represent tumours that are sensitive to fractionation and typically also slow-growing, while the second pair of values (α/β=17.59 Gy and μ=1.28 h^{-1}) is used to represent highly proliferative tumours which are less sensitive to fractionation. The proliferation rate parameterised in terms of doubling time (Dale, 1996) is not explicitly considered in this work, and the proliferative properties associated with different radiobiological parameters only reflect typical characteristics of tumours. For the liver, values of α/β and μ of 2.5 Gy and 0.28 h^{-1} respectively, are applied (Cremonesi *et al.*, 2008). Table I summarises the radiobiological and pharmacokinetic parameters used.

Table I. Radiobiological and pharmacokinetic parameters of tumour and liver used for calculations.

RADIOBIOLOGICAL PARAMETERS				
	Tumour		Liver	
	Case I_{Tum}	Case II_{Tum}	Case I_{Liv} and Case II_{Liv}	
α/β **[Gy]**	1.85	17.59	2.5	
μ **[h^{-1}]**	0.46	1.28	0.28	
PHARMACOKINETIC PARAMETERS				
	Tumour		Liver	
	Case I_{Tum} and Case II_{Tum}		Case I_{Liv}	Case II_{Liv}
D/A_{Adm} **[Gy/GBq]**	1.50		0.83	0.29
λ **[h^{-1}]**	0.008		0.025	0.009

The BED of tumour, BED_{Tum}, and of liver, BED_{Liv}, are calculated for the schedules of activity delivery shown in Figure 2, using the equations developed in this study and using previously published equation (6), for parameter values listed in Table I. In addition, the computer program developed by Gustafsson *et al.* (2013b), in which BED calculations are performed using a discrete convolution, is used for independent verification of results.

3. Results

3.1.Mathematical expression for BED in fractionated MRT

In Appendix A it is shown that for situations when repair is modelled by a monoexponential function, the time-dose-rate curve shows the same monoexponential behaviour in all administrations, and an equal amount of activity is given at equally spaced time intervals, Δ*t*, the expression for $G_{n,\infty}$ is given by:

$$G_{n,\infty} = \frac{\lambda}{n(\mu+\lambda)}\left\{1 + \frac{2}{n(\mu-\lambda)}\left[\mu f_n(\exp(-\lambda\Delta t)) - \lambda f_n(\exp(-\mu\Delta t))\right]\right\}, \tag{7}$$

where the function $f_n(x)$ is defined as

$$f_n(x) = \frac{x^n - nx + n - 1}{x - 2 + x^{-1}}. \tag{8}$$

Once $G_{n,\infty}$ is known, the BED can be calculated according to:

$$\text{BED} = D\left(1 + \frac{D}{\alpha/\beta}\, G_{n,\infty}\right). \tag{9}$$

It can be noted that BED in (9) depends on *D*, *λ*, *μ*, *α/β*, *n* and Δ*t*, while BED in (6) depends on the same parameters except for Δ*t*. From (4) and (7) it is seen that the first term in $G_{n,\infty}$ is identical to $G_{1,\infty}/n$, while the term within braces describes the increase in the G-factor due to interplay between absorbed-dose rate curves. In order to analyse the properties of the last term we define the function F_n according to:

$$F_n = \frac{G_{n,\infty}}{G_{1,\infty}/n} = 1 + \frac{2}{n(\mu-\lambda)}\left[\mu f_n(\exp(-\lambda\Delta t)) - \lambda f_n(\exp(-\mu\Delta t))\right]. \tag{10}$$

From (8) and (10) it is seen that $f_1(x)$ evaluates to zero, and F_1 evaluates to unity, which is thus consistent with (4) and (6).

In the majority of MRT, the repair half time is much shorter than the effective half-life of the radiopharmaceutical, i.e. $\mu >> \lambda$. The properties of (10) can be analysed by defining a variable $s = \mu/\lambda$, so that

$$\begin{aligned} F_n &= 1 + \frac{2}{n(s\lambda-\lambda)}\left[s\lambda f_n(\exp(-\lambda\Delta t)) - \lambda f_n(\exp(-s\lambda\Delta t))\right] \\ &= 1 + \frac{2}{n(s-1)}\left[s f_n(\exp(-\lambda\Delta t)) - f_n(\exp(-s\lambda\Delta t))\right]. \end{aligned} \tag{11}$$

Thus, it is seen that when $s >> 1$, F_n can be approximated as:

$$F_n \approx 1 + \frac{2}{n}\ f_n(\exp(-\lambda\Delta t)). \qquad (12)$$

The parameters that are most influential for F_n are n and the product $\lambda\Delta t$. Figure 3 shows F_n obtained from (10) and (12) as a function of $\lambda\Delta t$ for values of n = 1, 2, 4, 6 and 8. For (10) a value s of 58 is used, corresponding to values of μ and λ of 0.46 h^{-1} and 0.008 h^{-1}, respectively (case I_{Tum}). However, as long as $\mu >> \lambda$, F_n mainly depends on the relation between λ and Δt, as shown by results from Equation (12).

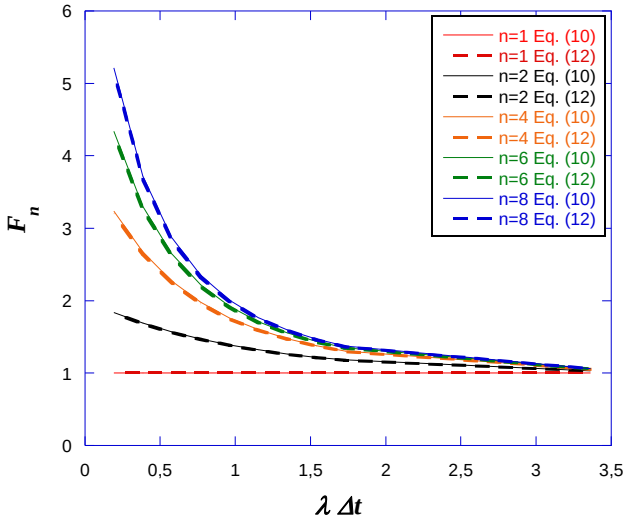

Figure 3. Values of F_n as a function of $\lambda\Delta t$ for n = 1, 2, 4, 6 and 8.

3.2.Application to fractionated ^{131}I-mIBG treatment of NB

Figure 4 shows BED_{Tum} as a function of Δt for case I_{Tum} (I_{Tum} : α/β=1.85 Gy, μ=0.46 h^{-1}, D/A_{Adm}=1.5 Gy/GBq and λ=0.008 h^{-1}), when two administrations, each of 28 GBq, are given. It is shown that, in this example, (6) and (9) give approximately the same BED for large Δt, but as Δt decreases, (9) gives higher values than (6). As Δt goes to zero, the BED obtained from (9) approaches the BED for a single-administration treatment (BED_{Tum} = 149.2 Gy), as calculated using (9) for n = 1, which is thus consistent. BED values from (6) are independent of Δt and thus do not approach the single-administration BED for short Δt.

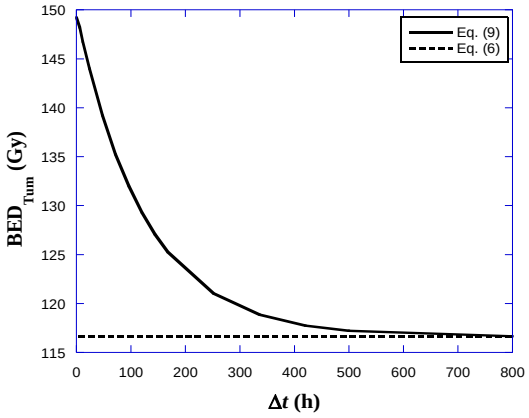

Figure 4. Values of BED_{Tum} as a function of Δt for case I_{Tum} calculated from (6) and (9) when two administrations, each of 28 GBq, are given. N. B. Values of the vertical axis do not start at 0.

Figure 5 shows values of BED_{Tum} for cases I_{Tum} and II_{Tum}, and values of BED_{Liv} for cases I_{Liv} and II_{Liv}, when (6) and (9) are used. When using (9) for cases I_{Tum} and I_{Liv} the BED decreases for schedules 2, 3 and 4 as compared to schedule 1, with maximum differences obtained of 12% and 29% (calculated as difference with regard to schedule 1) for cases I_{Tum} and I_{Liv}, respectively. For cases II_{Tum} and II_{Liv} the BED remains relatively constant for schedules 1, 2, 3 and 4, with maximum differences obtained of below 1% and 4%, for II_{Tum} and II_{Liv}, respectively. Comparing schedule 5 with schedule 1, the BED decreases with differences obtained of 47%, 58%, 47% and 50% for cases $I_{Tum,}$ I_{Liv}, II_{Tum} and $II_{Liv,}$ respectively. The differences between (6) and (9) are higher for the shorter time intervals between administrations, and in all cases (6) underestimates the BED, with differences obtained for schedule 4 (calculated as difference with regard to (9)) of 12.3%, 0.6%, 4.0% and 3.4%, for cases I_{Tum}, II_{Tum}, I_{Liv} and II_{Liv}, respectively.

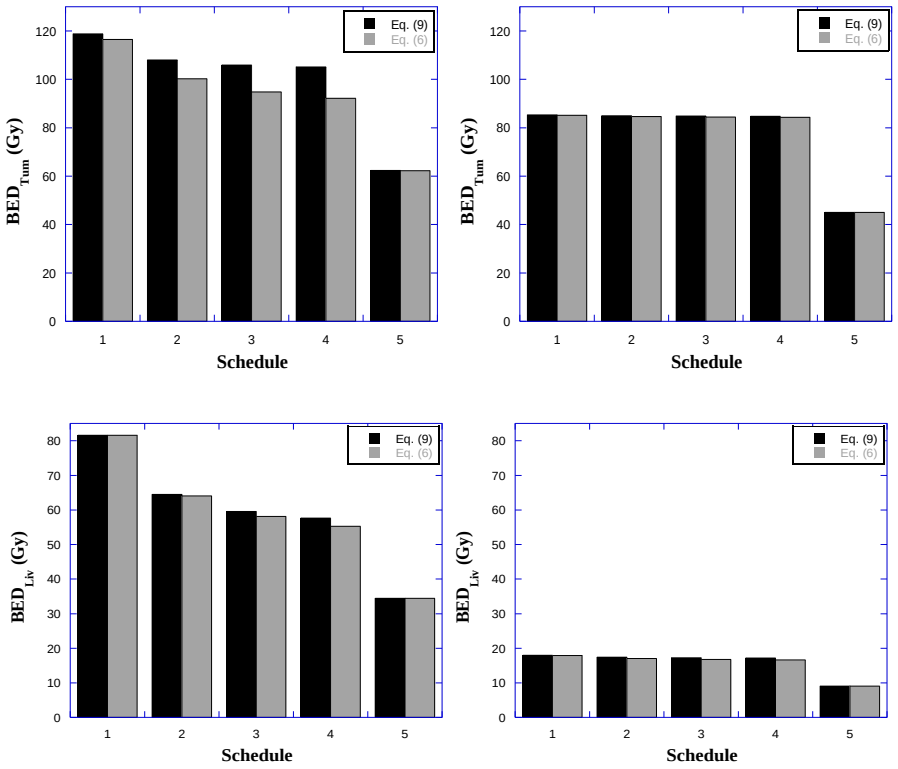

Figure 5. Values of BED_{Tum} and of BED_{Liv} for the five different schedules of activity delivery using (6) and (9) for cases I_{Tum} (top left) and II_{Tum} (top right) (I_{Tum} : α/β =1.85 Gy, μ= 0.46 h^{-1} ; II_{Tum} : α/β=17.59 Gy, μ = 1.28 h^{-1}); and for cases I_{Liv} (bottom left) and II_{Liv} (bottom right) (I_{Liv}: D/A_{Adm} = 0.83 Gy/GBq, λ = 0.025 h^{-1}; II_{Liv}: D/A_{Adm} = 0.29 Gy/GBq λ = 0.009 h^{-1}). (Schedule 1: 2×28 GBq. Schedule 2: 4×14 GBq. Schedule 3: 6×9.33 GBq. Schedule 4: 8×7 GBq. Schedule 5: 2×14.8 GBq).

The differences in BED obtained from using (9), and using methods described by Gustafsson *et al.* (2013b) are below 0.01% for all calculations performed, showing that the two methods for BED calculation are consistent.

4. Discussion

This study investigates the effects on BED of fractionation in MRT, in particular in NB treatments with ^{131}I-mIBG. For this purpose an expression for the Lea-Catcheside G-factor is derived, which in contrast to the previously used expression (Cremonesi *et al.*, 2006; Baechler *et al.*, 2008; Cremonesi *et al.*, 2008), includes the possibility that pairs of sublethal damage caused by radiation associated with different administrations combine into a lethal damage. As shown by (7) the function $G_{n,\infty}$ in the Lea-Catcheside G-factor integrated up to infinite time for n administrations, depends on λ, μ, n and Δt, while the formerly used equation (6), depends on the same parameters except for Δt. In (10) it is shown that a function F_n can be identified that constitutes the factor to which the formerly used expression, $G_{1,\infty}/n$, should be multiplied in order to give $G_{n,\infty}$. In (11) it is demonstrated that for the majority of MRT, where the repair half time is much shorter than the effective half-life of the radiopharmaceutical, i.e. $\mu >> \lambda$, the parameters that are most influential for F_n are n and the product $\lambda\Delta t$, and the approximative expression in (12) can then be applied. Figure 3 shows the values of F_n as a function of $\lambda\Delta t$, for different n. It is seen that if Δt is large, the function F_n evaluates to one, and $G_{n,\infty}$ thus equates $G_{1,\infty}/n$. When Δt decreases, F_n gradually increases. For instance, when Δt is in the order of $1/\lambda$, and a two-administration treatment is given, the function F_n evaluates to 1.5. F_n increases as function of n, mostly so for few administrations, while when using many administations F_n converges towards a value that is dependent on $\lambda\Delta t$. In clinical planning of fractionated MRT, parameters that need to be defined are n and Δt. Figure 3 can here be used to estimate the importance of F_n, and thus $G_{n,\infty}$, for different combinations of n and $\lambda\Delta t$.

The derivation in Appendix A starts with a general discussion about the properties of the G-factor for repeated, identical irradiation time-patterns without explicit assumptions on the particular form of the time-pattern, time separation, or choice of repair function. Further assumptions, e.g. equal time separations and a mono-exponentially decaying absorbed-dose rate, are introduced when needed. The adopted approach, starting from a general perspective, is believed to be useful since, potentially, the intermediate results may be applied also to other time-patterns or repair functions. Although the derivation is relatively long, we find that the final expression for the G-factor in (7) is surprisingly simple. This makes the formula practically useful for theoretical reasoning about the effects of fractionation in MRT.

The simplicity of the BED expression comes to the cost of some assumptions. In principle, the assumption of equidistant administrations with the same activity may limit its application, but it is noted that this is the aimed pattern in the schedule by Gaze *et al.* (2005), and also in other MRT, for instance using ^{177}Lu-DOTATATE (Delpassand *et al.*, 2014) and ^{223}Ra-chloride (Lassmann and Nosske, 2013). Although the practical application of the BED formula has been focussed on ^{131}I-mIBG, it can be applied to other types of fractionated MRT. Recently, different therapeutic schemes in ^{177}Lu-DOTATATE and ^{90}Y-DOTATOC MRT have been compared from a radiobiological

viewpoint (Sarnelli, 2015). Regarding the assumption of mono-exponential decaying absorbed-dose rate, this assumption is commonly made (Millar, 1991), although, in principle, it is often an approximation of a more complicated time-pattern. For a more complex situation where these assumptions do not apply one possibility would be to use numerical methods for calculating the BED (Gustafsson *et al.*, 2013b). Another limitation is that effects of proliferation have not been addressed, the main reason being that such effects would probably be similar between the investigated schedules of activity delivery given that the rate of repopulation is assumed to be modest, but also that data on such effects in MRT are highly limited.

As an example application of the derived expression for calculation of BED, different schedules for myeloablative ^{131}I-mIBG treatment of NB are analysed. The original motivation was a clinical situation when the activity to administer, calculated according to the schedule by Gaze *et al.* (2005), exceeded the maximum authorised activity limit of 14.8 GBq. For patients exceeding 33 kg, the prescription 444 MBq/kg can thus not be followed at the Gurutzeta-Cruces University Hospital. Although patients treated for NB usually have lower masses, in the study by Buckley *et al.* (2009), 5 out of 26 of the included patients (19%) had masses exceeding 33 kg. Thus, in facilities where there is an upper activity limit, additional fractionation may be an option in order to follow the total prescribed activity while still complying with local regulations.

As starting point for the BED analysis, data from a patient case, as well as literature values of pharmacokinetic and radiobiological parameters for liver and tumour are used. The choice of liver as the organ at risk is motivated by the inclusion of bone marrow support in the treatment, and observations of a sometimes high liver accumulation of ^{131}I-mIBG (Koral *et al.*, 2008). Comparisons of the BED (BED_{Tum} and BED_{Liv}) when calculated using the previously presented equation (6) and the new equation (9) are made for the original two-administration schedule (schedule 1) (Gaze *et al.*, 2005), as well as three schedules that include additional fractionation (schedules 2, 3 and 4) and a two-administration schedule with the maximum authorised activity (schedule 5). The difference in results for I_{Tum} and II_{Tum} is mainly governed by the α/β value used, and to a lesser extent by the μ value, whereas the difference between I_{Liv} and II_{Liv} is mainly governed by the values of D/A_{Adm} used. It is worth pointing out that the total administered activity in schedules 2, 3 and 4 is the same as in schedule 1, and that they would not interfere with the timing of the stem-cell rescue in the original schedule 1.

As shown by the differences obtained between cases I_{Tum} and II_{Tum} (Figure 5), the choice of radiobiological parameters affects the obtained values of BED_{Tum}. For tumours, values of α/β obtained from *in vitro* human NB cell lines are considered, since *in vivo* data could not be identified in the literature. To some extent this approach is supported by results in Carlson *et al.* (2004), where *in vitro* and *in vivo* α/β values for prostate cancer were compared and found to be consistent.

With regard to pharmacokinetic parameters, for liver two cases are studied, cases I_{Liv} and II_{Liv}, representing high and low liver accumulation of ^{131}I-mIBG, respectively. For

tumour tissue the analysis is limited to one set of values of D/A_{Adm} and λ, as determined for a patient (Appendix B), because of the shortage of paired data in the literature. Higher values of D/A_{Adm} would result in higher BED_{Tum} differences between the different schedules shown in Figure 5, and higher values of λ would result in higher differences in BED_{Tum}, for the shorter Δt, and in lower differences for the longer Δt.

The assumption that the biodistribution and pharmacokinetics of ^{131}I-mIBG is identical in subsequent administrations can be questioned, but is supported by observations in the literature (Wafelman *et al.*, 1994; Vallabhajosula and Nikolopoulou, 2011). Accumulation in cells of mIBG occurs by two processes: a specific and saturable uptake, and a non-specific and unsaturable uptake (Vallabhajosula and Nikolopoulou, 2011) and according to Wafelman *et al.* (1994), no saturation effects in the specific uptake have been observed for therapeutic doses of ^{131}I-mIBG. Moreover, in Minguez *et al.* (2015), similar whole-body absorbed doses were obtained in two and even three subsequent administrations.

In Figure 5 it is shown that when there is a maximum permitted activity per administration, one way of maintaining the protocol-prescribed total activity is to give additional fractions, causing only a small loss in BED_{Tum}. This is of relevance for current clinical treatments, where otherwise schedule 5 is commonly applied. It is also seen that the decrease in BED_{Tum} is modest when changing from two to eight activity administrations while maintaining the total activity, and the differences between schedules 2 to 4 are probably of minor importance given the current practice of MRT where a specific tumour absorbed dose or BED_{Tum} is normally not prescribed. Figure 5 also shows that the decrease in BED_{Tum} is accompanied by a decrease in BED_{Liv}. Hence, from the perspective of the liver, fractionation could allow for a higher total activity and thus a higher BED_{Tum}. This is of clinical relevance when aiming at optimising treatment protocols, starting from the perspective of radiobiological modelling (Sarnelli, 2015).

To analyse the theoretical consequences of different schedules of activity delivery, the ratio BED_{Tum} / BED_{Liv} can be studied to highlight the relationship between BED_{Tum} and BED_{Liv} when introducing fractionation. The ratio of BED_{Tum} to the BED of organs at risk has been suggested as a clinically useful metric to choose between different fractionation schemes in EBRT (Fowler, 2010). In MRT we believe that this BED-ratio may be interesting, since BED_{Tum} and the BED of organs at risk cannot be treated separately, but both depend on the amount of administered activity. The particular value of the ratio does not have a meaning in itself, but the change in the ratio for different schedules of activity delivery illustrates the consequences of changing schedules, in view of different values of radiobiological and pharmacokinetic parameters. For such an analysis to be useful, it is important that the trend in the BED ratio, in our case BED_{Tum} / BED_{Liv}, does not change with the total amount of administered activities for clinically relevant ranges. Figure 6 shows the ratio BED_{Tum} / BED_{Liv}, calculated for cases I_{Tum}−II_{Liv} and II_{Tum}−I_{Liv} for schedules 1-4 in Figure 2, and as a function of the administered activity.

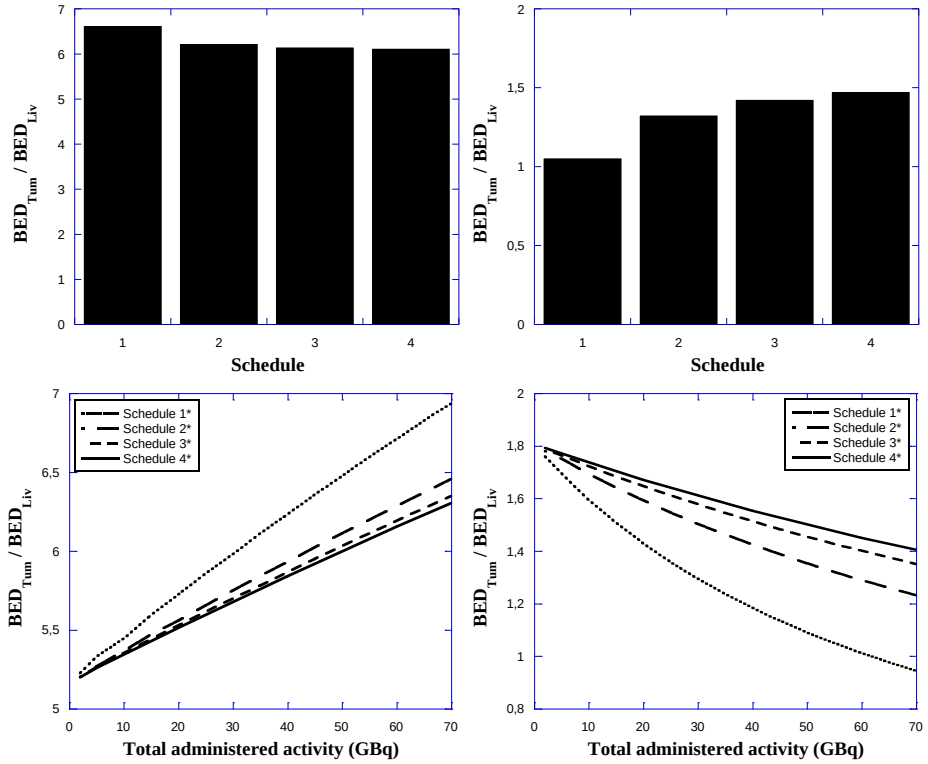

Figure 6. Values of BED_{Tum} / BED_{Liv} obtained using (9) for cases I_{Tum} - II_{Liv} (left) and II_{Tum}- I_{Liv} (right). Top panels show the ratio for schedules in Figure 2, while bottom panels show the ratio as function of the total administered activity, where the star indicates that the administered activity is not maintained as in Figure 2.

It is seen that in cases I_{Tum}–II_{Liv}, the ratio BED_{Tum} / BED_{Liv} gradually decreases in schedules 2, 3 and 4 with regard to schedule 1, mainly due to the decrease in BED_{Tum} for I_{Tum}, while BED_{Liv} for II_{Liv}, representing a low liver uptake, remains nearly constant (Figure 5). In the combination of cases II_{Tum}–I_{Liv} the ratio BED_{Tum} / BED_{Liv} increases in schedules 2, 3 and 4 with regard to schedule 1. The increase is mainly governed by the loss of BED_{Liv} for I_{Liv}, while BED_{Tum} for II_{Tum}, with a high α/β, is less sensitive to fractionation. As shown in the bottom panels, the value of the ratio depends on the administered activity, but the order of the different schedules does not change. Thus, if a therapy can be designed so as to keep the BED of an organ at risk at a constant level, the BED-ratio may be useful to analyse the possible consequences of fractionation. In our cases, if BED_{Liv} was to be kept constant, fractionation would imply a higher BED_{Tum} in cases II_{Tum}–I_{Liv} but a lower BED_{Tum} in cases I_{Tum}–II_{Liv}, and the possible gain or loss in BED_{Tum} would depend on the administered activity.

In the protocol by Gaze *et al*. (2005) for ^{131}I-mIBG treatment, a limit of the total whole-body absorbed dose of 4 Gy is applied, and the total amount of administered activity can thus not be increased. Therefore, the ratio in Figure 6 is not intended to change the administration protocol for this particular treatment, but merely to highlight and discuss the consequences of fractionation.

5. Conclusions

In this study, a formula for the Lea-Catcheside G-factor was developed to be applied for BED calculations in fractionated MRT. The new formula takes the possibility of interplay between the absorbed-dose rate curves resulting from different administrations into account. An approximate expression was also derived, showing that the differences between the previous and new expression are mainly governed by the number of administrations, and the product of the time interval between administrations and the effective decay constant of the radiopharmaceutical.

As example application, the BED of treatment was analysed in a two-administration schedule for NB treatments with ^{131}I-mIBG, in which the activity per administration exceeded the legally authorised activity. The introduction of additional fractionation resulted in a modest decrease in BED of tumour, in comparison to the BED decrease obtained when adjusting the administered activity to the authorised limit.

Acknowledgments

This work was supported by the Swedish Research Council (grant # 621-2014-6187), the Berta Kamprad Foundation and the Swedish Society for Radiation Physics.

Appendix A. Derivation of the Lea-Catcheside G-factor for fractionated MRT.

In this appendix, equation (7) will be derived. To begin with, some properties of BED for repeated, general absorbed-dose rate functions are formulated, as well as their relationship to BED for a single irradiation. These properties are then applied to the special case of fractionated MRT.

The general case

Denote the absorbed-dose rate as a function of time as $R(t)$ and the function describing repair of sublethal damages as $\varphi(t)$. Assume that $R(t)$ is composed of n identical absorbed-dose rate functions $r(t)$ that each is translated a time T_i, according to

$$R(t) = \sum_{i=0}^{n-1} r(t - T_i). \tag{A1}$$

The function $r(t)$ will henceforth be referred to as a fraction.

For notational convenience, define a zero-padded repair function, $I(t)$,

$$I(t) = \begin{cases} 0, & < t, \\ \varphi(t), & t \geq 0. \end{cases} \tag{A2}$$

Following Gustafsson *et al.* (2013a) the effects of repair can be modelled as a convolution between the functions R and I,

$$C(t) = R \otimes I. \tag{A3}$$

The Lea-Catcheside G-factor, can then be calculated as

$$G = \frac{2H}{D^2} = \frac{2H}{(nd)^2}, \tag{A4}$$

where D is the total absorbed dose, d is the absorbed dose from each fraction and

$$H = \int_{-\infty}^{\infty} R(t)C(t)\mathrm{d}t. \tag{A5}$$

The corresponding expressions for a single fraction, denoted by subscript p (for partial), are,

$$C_{\mathrm{p}}(t) = r \otimes I. \tag{A6}$$

$$H_{\mathrm{p}} = \int_{-\infty}^{\infty} r(t) C_{\mathrm{p}}(t) \mathrm{d}t, \tag{A7}$$

and

$$G_{\mathrm{p}} = \frac{2H_{\mathrm{p}}}{d^2}. \tag{A8}$$

Combining (A1), (A3) and (A6) gives that

$$C(t) = \sum_{i=0}^{n-1} C_{\mathrm{p}}(t - T_i). \tag{A9}$$

Inserting into (A5) leads to

$$\begin{aligned} H = \int_{-\infty}^{\infty} \sum_{i=0}^{n-1} r(t - T_i) \sum_{j=0}^{n-1} C_{\mathrm{p}}(t - T_j)\, \mathrm{d}t = \sum_{i=0}^{n-1} \sum_{j=0}^{n-1} \int_{-\infty}^{\infty} r(t - T_i) C_{\mathrm{p}}(t - T_j) \mathrm{d}t = \\ = \sum_{i=0}^{n-1} \sum_{j=0}^{n-1} \int_{-\infty}^{\infty} r(\tau - [T_i - T_j]) C_{\mathrm{p}}(\tau) \mathrm{d}\tau, \end{aligned} \tag{A10}$$

where a change of variables $\tau = t - T_j$ for each term has been performed in the last step.

The double sum in (A10) can be seen as a sum of elements in an $n \times n$ matrix where for each element i, j above the diagonal there is a corresponding element j, i below the diagonal. Define the time differences as $\Delta_{i,j} = T_i - T_j$. These differences have the properties $\Delta_{j,i} = -\Delta_{i,j}$ and $\Delta_{i,i} = 0$. The summation in (A10) can thus be simplified according to

$$\begin{aligned} H = \sum_{i=0}^{n-1} \int_{-\infty}^{\infty} r(\tau - \Delta_{i,i}) C_{\mathrm{p}}(\tau) \mathrm{d}\tau \\ + \sum_{i=1}^{n-1} \sum_{j=0}^{i-1} \left\{ \int_{-\infty}^{\infty} r(\tau - \Delta_{i,j}) C_{\mathrm{p}}(\tau) \mathrm{d}\tau + \int_{-\infty}^{\infty} r(\tau - \Delta_{j,i}) C_{\mathrm{p}}(\tau) \mathrm{d}\tau \right\} \\ = nH_{\mathrm{p}} + \sum_{i=1}^{n-1} \sum_{j=0}^{i-1} \left\{ \int_{-\infty}^{\infty} r(\tau - \Delta_{i,j}) C_{\mathrm{p}}(\tau) \mathrm{d}\tau + \int_{-\infty}^{\infty} r(\tau + \Delta_{i,j}) C_{\mathrm{p}}(\tau) \mathrm{d}\tau \right\}. \end{aligned} \tag{A11}$$

The first term in (A11) represents the contribution to G from sublethal damages that interact within a fraction, for which expressions for G_{p}, and hence H_{p}, can be found in standard literature for most common r. The second term, further on denoted as H_{c},

represents the contribution from cross-interaction of radiation sublethal damages between different fractions. G in (A4) can thus be expressed as

$$G = \frac{2\left(nH_{\mathrm{p}} + H_{\mathrm{c}}\right)}{(nd)^2} = \frac{G_{\mathrm{p}}}{n} + \frac{2H_{\mathrm{c}}}{(nd)^2}. \tag{A12}$$

The following derivation will focus on the expression of H_{c} for equidistant fractions.

Equidistant fractions

Assume that fractions are given at equal time intervals, Δt, e.g. $T_i = i \cdot \Delta t$. This causes the time differences to have the additional property of $\Delta_{i,j} = \Delta_{i+1,j+1}$. So, in the expression for H_{c} for every i there will be $n - i$ terms identical to the term $i, 0$. The double sum in (A11), can thus be evaluated according to

$$\begin{aligned} H_{\mathrm{c}} &= \sum_{i=1}^{n-1}(n-i)\left\{\int_{-\infty}^{\infty} r\left(\tau - \Delta_{i,0}\right)C_{\mathrm{p}}(\tau)\mathrm{d}\tau + \int_{-\infty}^{\infty} r\left(\tau + \Delta_{i,0}\right)C_{\mathrm{p}}(\tau)\mathrm{d}\tau\right\} \\ &= \sum_{i=1}^{n-1}(n-i)\left\{\int_{-\infty}^{\infty} r(\tau - i\Delta t)C_{\mathrm{p}}(\tau)\mathrm{d}\tau + \int_{-\infty}^{\infty} r(\tau + i\Delta t)C_{\mathrm{p}}(\tau)\mathrm{d}\tau\right\}. \end{aligned} \tag{A13}$$

Mono-exponential functions

For the specific case of fractionated MRT with monoexponentially decaying absorbed-dose rate functions, let

$$r(t) = \begin{cases} 0, & t < 0, \\ R_0 \exp(-\lambda t) & t \geq 0, \end{cases} \tag{A14}$$

where R_0 is the absorbed-dose rate at time zero, and λ is the effective decay constant. Also assume that repair follows mono-exponential kinetics with rate constant μ, i.e.

$$\varphi(t) = \exp(-\mu t) \;\; t \geq 0. \tag{A15}$$

This leads to

$$C_{\mathrm{p}}(t) = \begin{cases} 0, & t < 0, \\ \dfrac{R_0}{\mu - \lambda}\left[\exp(-\lambda t) - \exp(-\mu t)\right] & t \geq 0. \end{cases} \tag{A16}$$

Inserting into (A13) gives

$$\begin{aligned} H_{\mathrm{c}} &= \sum_{i=1}^{n-1}(n-i)\left\{\int_{i\Delta t}^{\infty} R_0 \exp(-\lambda[\tau - i\Delta t])\frac{R_0}{\mu - \lambda}\left[\exp(-\lambda\tau) - \exp(-\mu\tau)\right]\mathrm{d}\tau\right. \\ &\left. + \int_{0}^{\infty} R_0 \exp(-\lambda[\tau + i\Delta t])\frac{R_0}{\mu - \lambda}\left[\exp(-\lambda\tau) - \exp(-\mu\tau)\right]\mathrm{d}\tau\right\} \\ &= \frac{R_0^2}{\mu - \lambda}\sum_{i=1}^{n-1}(n-i)\left\{\frac{\exp(-\lambda i\Delta t)}{\lambda} - \frac{\exp(-\mu i\Delta t) + \exp(-\lambda i\Delta t)}{\mu + \lambda}\right\}. \end{aligned} \tag{A17}$$

This expression can be even further simplified. For this purpose, define $\theta = \exp(-\lambda\Delta t)$ and $\psi = \exp(-\mu\Delta t)$, so that

$$H_c = \frac{R_0^2}{\mu - \lambda}\sum_{i=1}^{n-1}(n-i)\left\{\frac{\theta^i}{\lambda} - \frac{\psi^i + \theta^i}{\mu + \lambda}\right\}. \tag{A18}$$

Make a variable change of the index of summation, $k = n - i$

$$H_c = \frac{R_0^2}{\mu - \lambda}\sum_{k=1}^{n-1} k\left\{\frac{\theta^n\theta^{-k}}{\lambda} - \frac{\psi^n\psi^{-k} + \theta^n\theta^{-k}}{\mu + \lambda}\right\}. \tag{A19}$$

It can be shown that for a constant $a \neq 1$

$$\sum_{i=1}^{n-1} ia^i = \frac{a - na^n + (n-1)a^{n+1}}{(1-a)^2}, \tag{A20}$$

which can be proven by noting that

$$(1-a)\sum_{i=1}^{n-1} ia^i = \sum_{i=1}^{n-1} ia^i - a\sum_{i=1}^{n-1} ia^i = \sum_{i=1}^{n-1} a^i - (n-1)a^n = \frac{a - a^n}{1-a} - (n-1)a^n. \tag{A21}$$

Using (A20) and some algebraic simplifications leads to

$$\begin{aligned} H_c &= \frac{R_0^2}{\mu - \lambda}\left\{\frac{\theta^n}{\lambda}\sum_{k=1}^{n-1} k\,(\theta^{-1})^k - \frac{\psi^n}{\mu + \lambda}\sum_{k=1}^{n-1} k\,(\psi^{-1})^k - \frac{\theta^n}{\mu + \lambda}\sum_{k=1}^{n-1} k\,(\theta^{-1})^k\right\} \\ &= \frac{R_0^2}{(\mu + \lambda)(\mu - \lambda)}\left\{\frac{\mu}{\lambda}\frac{\exp(-\lambda n\Delta t) - n\exp(-\lambda\Delta t) + n - 1}{\exp(-\lambda\Delta t) - 2 + \exp(\lambda\Delta t)}\right. \\ &\left. - \frac{\exp(-\mu n\Delta t) - n\exp(-\mu\Delta t) + n - 1}{\exp(-\mu\Delta t) - 2 + \exp(\mu\Delta t)}\right\}. \end{aligned} \tag{A22}$$

Define the function

$$f_n(x) = \frac{x^n - nx + n - 1}{x - 2 + x^{-1}}, \tag{A23}$$

so that

$$H_c = \frac{R_0^2}{(\mu + \lambda)(\mu - \lambda)}\left\{\frac{\mu}{\lambda}f_n(\exp(-\lambda\Delta t)) - f_n(\exp(-\mu\Delta t))\right\}. \tag{A24}$$

Inserting (A24) into (A12), the expressions for the absorbed dose, i.e. $d = R_0/\lambda$, and G_p for a mono-exponential function combined with a mono-exponential repair function, i.e. $G_{1,\infty}$ in (5) in the Methods section, leads to

$$\begin{aligned} G_{n,\infty} &= \frac{G_{1,\infty}}{n} + \frac{2H_c}{(nd)^2} \\ &= \frac{\lambda}{n(\mu+\lambda)} + \frac{2\lambda^2}{n^2(\mu+\lambda)(\mu-\lambda)}\left\{\frac{\mu}{\lambda} f_n(\exp(-\lambda\Delta t)) - f_n(\exp(-\mu\Delta t))\right\} \\ &= \frac{\lambda}{n(\mu+\lambda)}\left\{1 + \frac{2}{n(\mu-\lambda)}[\mu f_n(\exp(-\lambda\Delta t)) - \lambda f_n(\exp(-\mu\Delta t))]\right\}, \end{aligned} \tag{A25}$$

which is the sought relationship.

Appendix B. Tumour and liver dosimetry.

Image-based dosimetry for tumour and liver was performed using a hybrid planar-SPECT/CT method (Koral *et al.*, 2000). Patient acquisitions were performed by planar anterior-posterior whole-body imaging at 46 h and 114 h post-administration, and SPECT/CT imaging at 114 h. A dual-head General Electric (GE, Fairfield, CT, USA) Infinia Hawkeye gamma camera was used, with a crystal thickness of 9.5 mm and equipped with high energy general purpose collimators. Planar imaging was performed using a scan speed of 12 cm/min, a matrix size of 256×1024, and a pixel size of 0.22 cm. SPECT projections were acquired in 60 angles, each of 60 s, using a matrix size of 128×128 and a pixel size of 0.44 cm. A 20% energy window centred at 364 keV was used.

The SPECT calibration factor was measured using an elliptically shaped phantom of approximately 4 litres which was filled with a known amount of activity (Dewaraja *et al.*, 2012). SPECT acquisitions were performed as described above, although for the phantom an additional 20% energy window centred at 297 keV was also used. SPECT image reconstruction was performed using the ordered subsets expectation maximization algorithm in a GE Xeleris work station, using 2 iterations and 10 subsets. CT-based attenuation correction was included for both patients and the calibration phantom. In phantom SPECT reconstructions, scatter correction was performed using the dual-energy-window method in the GE Infinia Hawkeye system. For patient images, where the scatter energy-window data were not available, scatter correction was performed by a phantom-derived scatter factor. This factor was derived from the phantom SPECT images, when reconstructed with and without scatter correction.

The SPECT calibration factor was determined as the total number of counts in a volume corresponding to the phantom. This value was divided by the acquisition time and the contained activity, thus giving the calibration factor in unit of cps/MBq. The patient SPECT/CT images were processed by manually delineating volumes of interest (VOIs) around tumour and liver in fused images, and determining the activity by dividing the SPECT VOI count rate by the calibration factor. From a relationship of the mass density versus the CT number, previously determined using a CT calibration phantom, the tumour and liver masses were determined from CT images as the mass density multiplied by the volumes.

The time-activity curve was determined from the planar images. Regions of interest (ROIs) were delineated over tumour and liver and the geometric mean of the ROI count rates calculated. Background correction was included by delineating equally sized ROIs near the tumour or liver, and avoiding any visible uptake. For attenuation correction, the extension of the tumour and liver in the anterior-posterior direction, and the patient thickness in these regions, were measured in CT images. The tumour and liver activities determined from the SPECT/CT image acquired at 114 h was used to renormalize the time-count rate curve determined from the planar images. The cumulated activity was determined by integration of this renormalized time-activity curve, and the absorbed

dose was calculated using mass-corrected S-values (Stabin *et al.*, 2005; Buckley *et al.*, 2007).

References

Amin A E, Wheldon T E, O'Donoghue J A, Gaze M N and Barrett A 1995 Optimum combination of targeted 131I and total body irradiation for treatment of disseminated cancer *Int. J. Radiat. Oncol. Biol. Phys.* **32** 713-21

Baechler S, Hobbs R F, Prideaux A R, Wahl R L and Sgouros G 2008 Extension of the biological effective dose to the MIRD schema and possible implications in radionuclide therapy dosimetry *Med. Phys.* **35** 1123-34

Barendsen G W 1982 Dose fractionation, dose rate and iso-effect relationships for normal tissue responses *Int. J. Radiat. Oncol. Biol. Phys.* **8** 1981-97

Barone R, Borson-Chazot F, Valkema R, Walrand S, Chauvin F, Gogou L, Kvols L K, Krenning E P, Jamar F and Pauwels S 2005 Patient-specific dosimetry in predicting renal toxicity with (90)Y-DOTATOC: relevance of kidney volume and dose rate in finding a dose-effect relationship *J. Nucl. Med.* **46 Suppl 1** 99S-106S

Brenner D J and Hall E J 1991 Conditions for the equivalence of continuous to pulsed low dose rate brachytherapy *Int. J. Radiat. Oncol. Biol. Phys.* **20** 181-90

Buckley S, Chittenden S, Saran F, Meller S and Flux G 2009 Whole-Body Dosimetry for Individualized Treatment Planning of 131I-MIBG Radionuclide Therapy for Neuroblastoma *J. Nucl. Med.***50** 1518-24

Buckley S E, Saran F H, Gaze M N, Chittenden S, Partridge M, Lancaster D, Pearson A and Flux G D 2007 Dosimetry for fractionated (131)I-mIBG therapies in patients with primary resistant high-risk neuroblastoma: preliminary results *Cancer Biother. Radiopharm.* **22** 105-12

Carlson D J, Stewart R D, Li X A, Jennings K, Wang J Z and Guerrero M 2004 Comparison of in vitro and in vivo alpha/beta ratios for prostate cancer *Phys. Med. Biol.* **49** 4477-91

Courdi A, Bensadoun R J, Gioanni J and Caldani C 1992 Inherent radiosensitivity and split-dose recovery in plateau-phase cultures of 10 human tumour cell lines *Radiother. Oncol.* **24** 102-7

Cremonesi M, Ferrari M, Bartolomei M, Orsi F, Bonomo G, Arico D, Mallia A, De Cicco C, Pedroli G and Paganelli G 2008 Radioembolisation with 90Y-microspheres: dosimetric and radiobiological investigation for multi-cycle treatment *Eur. J. Nucl. Med. Mol. Imaging* **35** 2088-96

Cremonesi M, Ferrari M, Bodei L, Tosi G and Paganelli G 2006 Dosimetry in Peptide radionuclide receptor therapy: a review *J. Nucl. Med.* **47** 1467-75

Dale R and Carabe-Fernandez A 2005 The radiobiology of conventional radiotherapy and its application to radionuclide therapy *Cancer Biother. Radiopharm.* **20** 47-51

Dale R G 1986 A graphical method to simplify the application of the linear-quadratic dose-effect equation to fractionated radiotherapy *Br. J. Radiol.* **59** 1111-5

Dale R G 1990 The use of small fraction numbers in high dose-rate gynaecological afterloading: some radiobiological considerations *Br. J. Radiol.* **63** 290-4

Dale R G 1996 Dose-rate effects in targeted radiotherapy *Phys. Med. Biol.* **41** 1871-84

Delpassand E S, Samarghandi A, Zamanian S, Wolin E M, Hamiditabar M, Espenan G D, Erion J L, O'Dorisio T M, Kvols L K, Simon J, Wolfangel R, Camp A, Krenning E P and Mojtahedi A 2014 Peptide receptor radionuclide therapy with 177Lu-DOTATATE for patients with somatostatin receptor-expressing neuroendocrine tumors: the first US phase 2 experience *Pancreas* **43** 518-25

Dewaraja Y K, Frey E C, Sgouros G, Brill A B, Roberson P, Zanzonico P B and Ljungberg M 2012 MIRD pamphlet No. 23: quantitative SPECT for patient-specific 3-dimensional dosimetry in internal radionuclide therapy *J. Nucl. Med.* **53** 1310-25

Dewaraja Y K, Schipper M J, Roberson P L, Wilderman S J, Amro H, Regan D D, Koral K F, Kaminski M S and Avram A M 2010 131I-tositumomab radioimmunotherapy: initial tumor dose-response results using 3-dimensional dosimetry including radiobiologic modeling *J. Nucl. Med.* **51** 1155-62

Fertil B and Malaise E P 1985 Intrinsic radiosensitivity of human cell lines is correlated with radioresponsiveness of human tumors: analysis of 101 published survival curves *Int. J. Radiat. Oncol. Biol. Phys.* **11** 1699-707

Fowler J F 1989 The linear-quadratic formula and progress in fractionated radiotherapy *Br. J. Radiol.* **62** 679-94

Fowler J F 1990 Radiobiological aspects of low dose rates in radioimmunotherapy *Int. J. Radiat. Oncol. Biol. Phys.* **18** 1261-9

Fowler J F 2010 21 years of biologically effective dose *Br. J. Radiol.* **83** 554-68

Gaze M N, Chang Y C, Flux G D, Mairs R J, Saran F H and Meller S T 2005 Feasibility of dosimetry-based high-dose 131I-meta-iodobenzylguanidine with topotecan as a radiosensitizer in children with metastatic neuroblastoma *Cancer Biother. Radiopharm.***20** 195-9

Gedik G K, Hoefnagel C A, Bais E and Olmos R A 2008 131I-MIBG therapy in metastatic phaeochromocytoma and paraganglioma *Eur. J. Nucl. Med. Mol. Imaging* **35** 725-33

Giammarile F, Chiti A, Lassmann M, Brans B and Flux G 2008 EANM procedure guidelines for 131I-meta-iodobenzylguanidine (131I-mIBG) therapy *Eur. J. Nucl. Med. Mol. Imaging* **35** 1039-47

Gustafsson J, Nilsson P and Sjögreen Gleisner K 2013a On the biologically effective dose (BED)-using convolution for calculating the effects of repair: I. Analytical considerations *Phys. Med. Biol.* **58** 1507-27

Gustafsson J, Nilsson P and Sjögreen Gleisner K 2013b On the biologically effective dose (BED)-using convolution for calculating the effects of repair: II. Numerical considerations *Phys. Med. Biol.* **58** 1529-48

Holmes A, McMillan T J, Peacock J H and Steel G G 1990 The radiation dose-rate effect in two human neuroblastoma cell lines *Br. J. Cancer* **62** 791-5

Howell R W, Goddu S M and Rao D V 1994 Application of the linear-quadratic model to radioimmunotherapy: further support for the advantage of longer-lived radionuclides *J. Nucl. Med.* **35** 1861-9

Jacobsson L M S, Johansson L, Lindberg S and Fjalling M 1985 Biokinetics and dosimetry of 131-I-metaiodobenzylguanidine (MIBG) *Proceeding of the Fourth International Radiopharmaceutical Dosimetry Symposium. Oak Ridge, TN.* 389-98

Kellerer A M and Rossi H H 1974 Current Topics in Radiation Research ed M Ebert and A Howard (Amsterdam:North-Holland) vol 8 pp 85–158

Koral K F, Dewaraja Y, Li J, Barrett C L, Regan D D, Zasadny K R, Rommelfanger S G, Francis I R, Kaminski M S and Wahl R L 2000 Initial results for Hybrid SPECT--conjugate-view tumor dosimetry in 131I-anti-B1 antibody therapy of previously untreated patients with lymphoma *J. Nucl. Med.* **41** 1579-86

Koral K F, Huberty J P, Frame B, Matthay K K, Maris J M, Regan D, Normolle D and Yanik G A 2008 Hepatic absorbed radiation dosimetry during I-131 metaiodobenzylguanidine (MIBG) therapy for refractory neuroblastoma *Eur. J. Nucl. Med. Mol. Imaging* **35** 2105-12

Lassmann M and Nosske D 2013 Dosimetry of 223Ra-chloride: dose to normal organs and tissues *Eur. J. Nucl. Med. Mol. Imaging* **40** 207-12

Lea D E and Catcheside D G 1942 The mechanism of the induction by radiation of chromosome aberrations in Tradescantia *J. Genet.* **44** 216-45

Malaise E P, Fertil B, Deschavanne P J, Chavaudra N and Brock W A 1987 Initial slope of radiation survival curves is characteristic of the origin of primary and established cultures of human tumor cells and fibroblasts *Radiat. Res.* **111** 319-33

Marchese M J, Zaider M and Hall E J 1987 Potentially lethal damage repair in human cells *Radiother. Oncol.* **9** 57-65

Millar W T 1991 Application of the linear-quadratic model with incomplete repair to radionuclide directed therapy *Br. J. Radiol.* **64** 242-51

Minguez P, Flux G, Genolla J, Guayambuco S, Delgado A, Fombellida J C and Sjögreen Gleisner K 2015 Dosimetric results in treatments of neuroblastoma and neuroendocrine

tumors with (131)I-metaiodobenzylguanidine with implications for the activity to administer *Med. Phys.* **42** 3969-78

Otte A, Herrmann R, Heppeler A, Behe M, Jermann E, Powell P, Maecke H R and Muller J 1999 Yttrium-90 DOTATOC: first clinical results *Eur. J. Nucl. Med.* **26** 1439-47

Quach A, Ji L, Mishra V, Sznewajs A, Veatch J, Huberty J, Franc B, Sposto R, Groshen S, Wei D, Fitzgerald P, Maris J M, Yanik G, Hawkins R A, Villablanca J G and Matthay K K 2011 Thyroid and hepatic function after high-dose 131 I-metaiodobenzylguanidine (131 I-MIBG) therapy for neuroblastoma *Pediatr. Blood Cancer* **56** 191-201

Sarnelli A, Guerriero F, Botta F, Ferrari M, Strigari L, Bodei L, D'Errico V, Grassi E, Fiorini F and Cremonesi M 2015 Therapeutic schemes in 177Lu and 90Y-PRRT:radiobiological considerations *Q. J. Nucl. Med. Mol. Imaging* (Epub Ahead of print)

Stabin M G, Sparks R B and Crowe E 2005 OLINDA/EXM: the second-generation personal computer software for internal dose assessment in nuclear medicine *J. Nucl. Med.* **46** 1023-7

Strigari L, Benassi M, Chiesa C, Cremonesi M, Bodei L and D'Andrea M 2011 Dosimetry in nuclear medicine therapy: radiobiology application and results *Q. J. Nucl. Med. Mol. Imaging* **55** 205-21

Strigari L, Konijnenberg M, Chiesa C, Bardies M, Du Y, Sjögreen Gleisner K, Lassmann M and Flux G 2014 The evidence base for the use of internal dosimetry in the clinical practice of molecular radiotherapy *Eur. J. Nucl. Med. Mol. Imaging* **41** 1976-88

Strigari L, Sciuto R, Rea S, Carpanese L, Pizzi G, Soriani A, Iaccarino G, Benassi M, Ettorre G M and Maini C L 2010 Efficacy and toxicity related to treatment of hepatocellular carcinoma with 90Y-SIR spheres: radiobiologic considerations *J. Nucl. Med.* **51** 1377-85

Sudbrock F, Schmidt M, Simon T, Eschner W, Berthold F and Schicha H 2010 Dosimetry for 131I-MIBG therapies in metastatic neuroblastoma, phaeochromocytoma and paraganglioma *Eur. J. Nucl. Med. Mol. Imaging* **37** 1279-90

Vallabhajosula S and Nikolopoulou A 2011 Radioiodinated metaiodobenzylguanidine (MIBG): radiochemistry, biology, and pharmacology *Semin. Nucl. Med.* **41** 324-33

Wafelman A R, Hoefnagel C A, Maes R A and Beijnen J H 1994 Radioiodinated metaiodobenzylguanidine: a review of its biodistribution and pharmacokinetics, drug interactions, cytotoxicity and dosimetry *Eur. J. Nucl. Med.* **21** 545-59

Yanik G A, Levine J E, Matthay K K, Sisson J C, Shulkin B L, Shapiro B, Hubers D, Spalding S, Braun T, Ferrara J L and Hutchinson R J 2002 Pilot study of iodine-131-metaiodobenzylguanidine in combination with myeloablative chemotherapy and autologous stem-cell support for the treatment of neuroblastoma *J. Clin. Oncol.* **20** 2142-9